Comparison of Dynamic Characteristics between Small and Super-Large Diameter Cross-River Twin Tunnels under Train Vibration

Lin Wu [1], Xiedong Zhang [1], Wei Wang [1,*], Xiancong Meng [1] and Hong Guo [2]

[1] School of Transportation and Logistics Engineering, Wuhan University of Technology, Wuhan 430063, China; wl256724@whut.edu.cn (L.W.); zhangxd@whut.edu.cn (X.Z.); mengxiancong@whut.edu.cn (X.M.)

[2] School of Civil Engineering and Architecture, Shaanxi University of Technology, Hanzhong 723001, China; hguo@snut.edu.cn

* Correspondence: wwei5633@whut.edu.cn; Tel.: +86-187-1133-2003

Featured Application: The quantitative comparison of the dynamic characteristics between super-large and small diameter twin tunnels under train vibration is helpful to the design and construction of super-large diameter twin tunnels.

Abstract: Train vibration from closely aligned adjacent tunnels could cause safety concerns, especially given the soaring size of the tunnel diameter. This paper established a two-dimensional discrete element model (DEM) of small (d = 6.2 m) and super-large (D = 15.2 m) diameter cross-river twin tunnels and discussed the dynamic characteristics of adjacent tunnels during the vibration of a train that runs through the tunnel at a speed of 120 km/h. Results in the D tunnel showed that the horizontal walls have the same horizontal displacement (D_H) and the vertical walls have the same vertical displacement (D_V). The stress state of the surroundings of the D tunnel is the decisive factor for D_H, and the distance from the vibration point to the measurement point is the decisive factor for D_V. Results in the comparison of the d and D tunnels showed that the D tunnel is more stable than the d tunnel with respect to two aspects: the time the tunnel reaches the equilibrium state and the vibration amplitude of the structure's dynamic and static responses. The dynamic characteristic of the d and D tunnel is significantly different. This research is expected to guide the design and construction of large diameter twin tunnels.

Keywords: twin tunnels; super-large diameter tunnel; train vibration load; dynamic characteristics; discrete element method (DEM)

1. Introduction

With the increasing shortage of underground space in cities, large diameter twin tunnels with near distances (i.e., smaller than 0.25 times diameter) are becoming more common. During tunnel operation, the vibration of a high-speed train disturbs the tunnel where the train runs and affects the structural stability and the train operation safety of the near-spacing adjacent tunnel.

The diameter of the tunnel is the main characteristic that will affect the behavior of the tunnel. Therefore, the research of tunnels can classify various tunnels by the size of the tunnel's diameter. There are many tunnels with a diameter of d_1 = 5–10 m under train vibration [1–3]. Studies with diameters between 10 and 15 m mainly focus on the construction stage of the tunnel [4–6]. The research focused on diameter $d_3 \geq 15$ m tunnels is inadequate. Studies focus only on the construction process of $d_3 \geq 15$ m tunnels [7,8] and the seismic characteristics of $d_3 \geq 15$ m tunnels during their operation period [9–11]. The dynamic characteristics of $d_3 \geq 15$ m cross-river twin tunnels under train vibration are different from those of small diameter twin tunnels. However, there are still few pieces

of research on the dynamic characteristics of a $d_3 \geq 15$ m tunnel under the vibration of a high-speed trains during tunnel operation. It is necessary to conduct specialized research on $d_3 \geq 15$ m twin tunnels, especially under train vibration.

In the study of train vibration in a single tunnel, Huang et al. [12] found that the final settlement of the subway tunnel in the saturated clay layer could reach 80 mm due to repeated train vibration. Yang et al. [13] found that the 2.5-dimensional numerical model of the soil-tunnel system under a moving train load was more accurate than the 2-dimensional model. He et al. [14,15] conducted a series of studies on the dynamic response of a single tunnel under train vibration load by using analytical methods and both 2.5-dimension and 3-dimension numerical methods. Yang et al. conducted a systematic study on the dynamic characteristics of single tunnel structure and its surroundings under train operation vibration [16,17]. Zhang et al. used DEM to study the dynamic characteristics of tunnel segments and surrounding rocks under train vibration in a single tunnel [1,18].

Studies on train vibration in twin tunnels are as follows. Ding et al. studied the influence of precision instruments in nearby laboratories under the vibration of Beijing Metro Line 8 and Line 15 [19]. He and Yan conducted a series of studies on the vibration response of trains under parallel-twin tunnels [20] and crossed twin tunnels [21]. Zhao et al. [22] studied the impact of high-speed train vibration loads on nearby damaged tunnels. It is necessary to re-construct and anchor the damaged tunnel to ensure the tunnel's safety. He et al. [23] established a 2.5-dimensional model that can predict train-induced vibration in tunnels with any cross-section. After that, He et al. [24] further proposed a three-dimensional analytical model for the interaction of subway vibration in parallel double tunnels. Zhou et al. [25] found that adjacent tunnels and water saturation had significant effects on soil vibration under subway vibration.

From the research on train vibration in single and twin tunnels, closely spaced twin tunnels (smaller than 0.25 times diameter) have become more common. In contrast, the research on train vibration has mainly focused on single tunnels. The research on train vibration has rarely focused on twin tunnels, and has especially neglected twin tunnels with a distance smaller than 0.25 times diameter.

This paper took the San-yang Road cross-river twin tunnels as the project background and established the small diameter ($d = 6.2$ m) and super-large diameter ($D = 15.2$ m) twin tunnels model by DEM. A train vibration load of 120 km/h in the first tunnel was simulated by several functions changing with time. In the first part, displacement and velocity of smoke exhaust board (Wall_1), vehicle lane board (Wall_2), left and right partition of train track (Wall_3 and Wall_4) in D adjacent tunnel were discussed In the second part, the displacement and velocity of sleepers and liners between the d and D adjacent tunnels were compared. The above analysis can be used to quantitatively compare the dynamic characteristics of super-large ($D = 15.2$ m) and small ($d = 6.2$ m) diameter twin tunnels under train vibrations.

2. Project Background and Type A Train

The project background of super-large diameter ($D = 15.2$ m) twin tunnels is the cross-river twin tunnels of San-yang Road in Wuhan Metro Line 7, as shown in Figure 1 [26]. The San-yang Road cross-river twin tunnels are used for urban road, and rail transit line 7 is the largest shield tunnel in China. The primary parameters of super-large diameter twin tunnels are 0.5 D buried depths, 1.0 D water depths, and 0.25 D spacing between the twin tunnels. The tunnel surroundings are silty sand, whose physical and mechanical parameters are shown in Table 1.
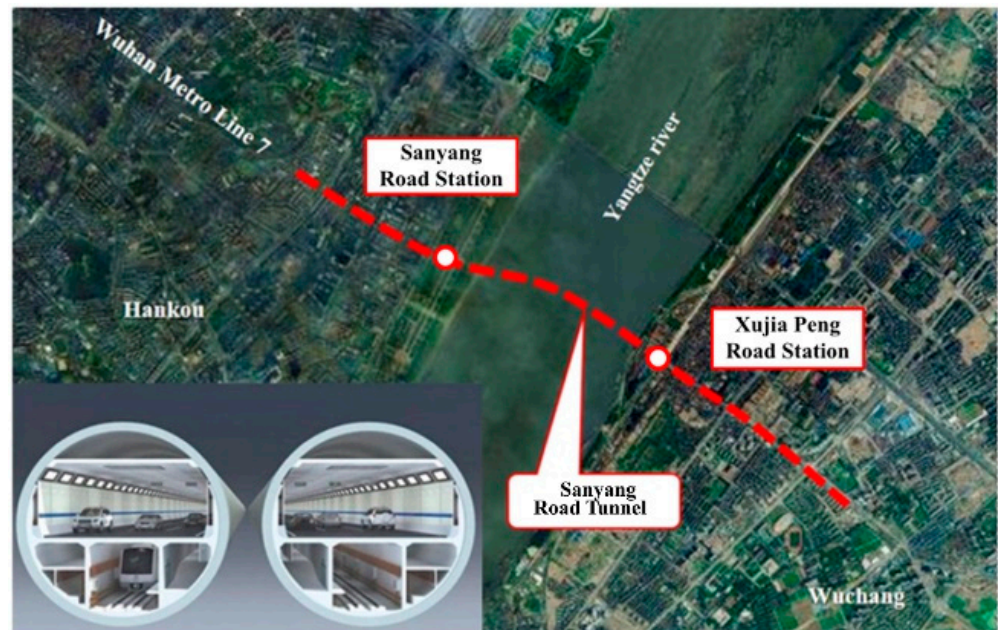
Figure 1. San-yang Road Yangtze River tunnel in Wuhan Metro Line 7.

Table 1. Physical and mechanical parameters of silty sand.

Silty Sand	w/%	E_s/MPa	c/kPa	φ/$^\circ$	v	γ/kN/m^3
Physical and mechanical parameters	20.4	21.9	7.0	31.9	0.49	20

Note: w is the water content; E_s is the compression modulus; c is the cohesion; φ is the friction; v is the Poisson's ratio; γ is the bulk density.

A supposed small diameter (d = 6.2 m) twin tunnels model was established compared with the D twin tunnels. The basic parameters are 0.5 d buried depths, 1.0 d water depths, and 0.25 d spacing between twin tunnels.

The primary parameter and the train vibration load of type A train are shown in Figure 2. The vibration load of carriages 2–5 is the same, and the load on the train head mirrors a load of train tail. The details of the train vibration load are shown in Formula (1) [3].

$$
\begin{aligned}
F_1 &= F_0[\cos(2\pi f_1 t) - 1] \\
F_2 &= -\frac{F_0}{5}[\cos(2\pi f_2 t) + 9] \\
F_3 &= -F_0[\cos(2\pi f_3 t) + 1] \\
F_4 &= -\frac{2F_0}{5}[\cos(2\pi f_4 t) + 4]
\end{aligned}
\tag{1}
$$

where F_1 is the function of the front spindle box of the first wheel; F_2 is a function of the distance between adjacent wheels; F_3 is a function of the middle part of the train; F_4 is the buoyancy box function of adjacent cars; $f_1, f_2, f_3,$ and f_4 are the frequencies of these functions, and t is the running time of the train (considering the dynamic characteristics of train operation, F_0 at 120 km/h is 31,221 N) [27].
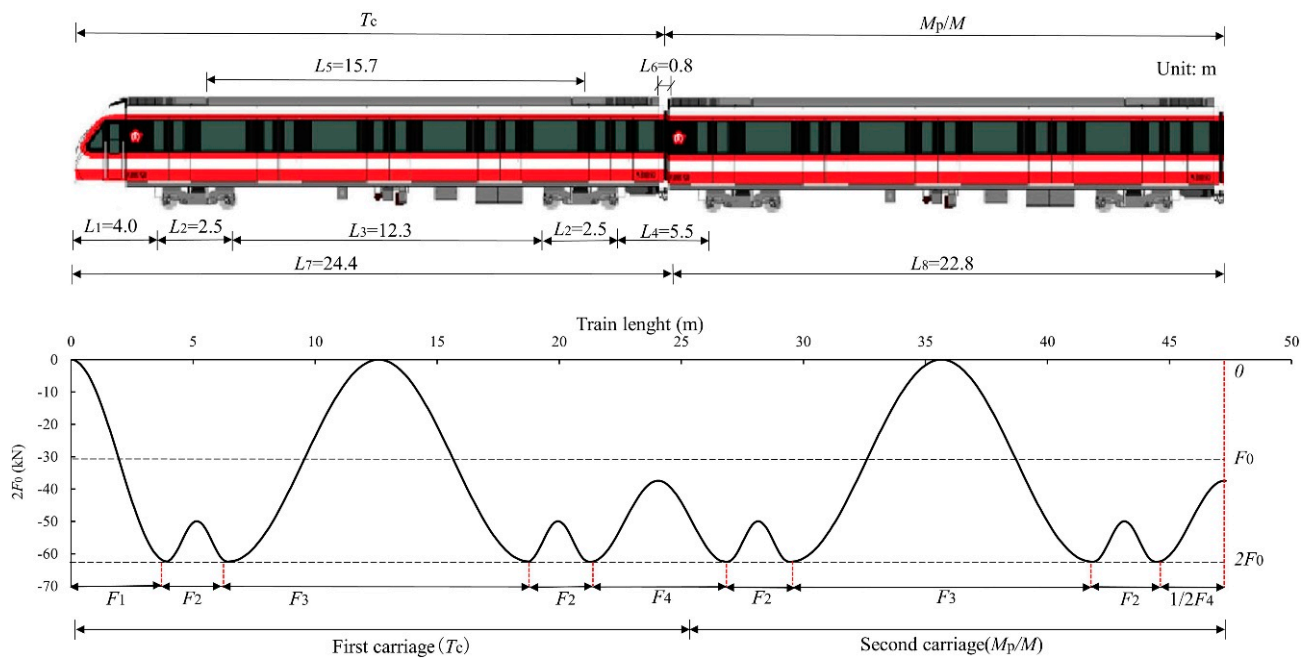
Figure 2. Vibration load caused by type A trains running at 120 km/h.

3. Micro-Parameters of Silty Sand and C60 Concrete

The calibration process is necessary for determining the micro-parameters of tunnel structure and surroundings in DEM. The tunnel structure contains walls, sleepers, and liners constructed by C60 concrete and the surroundings are silty sand. The size of particles in DEM affects the micro-parameters of silty sand and C60 concrete. Three sizes of silty sand (Table 2) and two sizes of C60 concrete (Table 3) have been calibrated in this section.

Table 2. Micro-parameters of silty sand in the DEM model.

Parameters	R (m)	ρ/kg/m^3	E_c/Pa	k^*	μ
Silty sand①	$R_1 = 0.12$–0.2	2000	2.05×10^7	1.0	0.62
Silty sand②	$R_2 = r_1 = 0.06$–0.1	2000	2.19×10^7	1.0	0.63
Silty sand③	$r_2 = 0.03$–0.05	2000	2.27×10^7	1.0	0.63

Note: R is the radius of particles; ρ is the density; E_c is the contact Young's modulus; k^* is the ratio of contact normal to shear stiffness; and μ is the coefficient of friction.

Table 3. Micro-parameters of C60 in the DEM model.

Parameters	C60①	C60②	Parameters	C60①	C60②
R (m)	$r_3 = 0.009$–0.012	$R_3 = 0.02$–0.03	T_N (MPa)	1.0×10^{100}	1.0×10^{100}
ρ (kg/m^3)	2500	2500	T_S (MPa)	1.0×10^{100}	1.0×10^{100}
E_c (Pa)	3.65×10^{10}	3.55×10^{10}	$\overline{E_C}$ (Pa)	3.65×10^{10}	3.55×10^{10}
k^*	1.0	1.0	$\overline{k^*}$	1.0	1.0
μ	0.84	0.85	$\overline{R}$	1.0	1.0

Note: C60① is for small diameter ($d = 6.2$ m) twin tunnels and C60② is for super-large diameter ($D = 15.2$ m) twin tunnels; R is the radius of particles; ρ is the density; E_c is the contact Young's modulus; k^* is the ratio of contact normal to shear stiffness; μ is the coefficient of friction; T_N is the normal strength of parallel bond; T_S is the tangential strength of parallel bond; and $\overline{E_C}$ is the contact Young's modulus of parallel bond; $\overline{k^*}$ is the ratio of parallel bond contact normal to shear stiffness; $\overline{R}$ is the parallel bonding radius.

The calibration process of silty sand② is as follows. First, two kinds of sand were mixed for the laboratory direct shear test for the shear force-strain curve of silty sand. By trial and error, 35% of Sand_1 and 65% of Sand_2 were used to obtain silty sand's physical and mechanical parameters (Figure 3). Second, the initial and final states of the shear test box were established in DEM (Figure 4) and normal stiffness, tangential

stiffness, and coefficient of friction were adjusted to obtain the stress-shear displacement ratio curve, which coincides with the curve obtained by laboratory direct shear test as shown in Figure 5. Finally, the microscopic parameters of silty sand② were used in the twin tunnel model in Section 4. The calibration process of other sizes of silty sand are similar, and the micro-parameters of silty sand ①–③ are shown in Table 2.
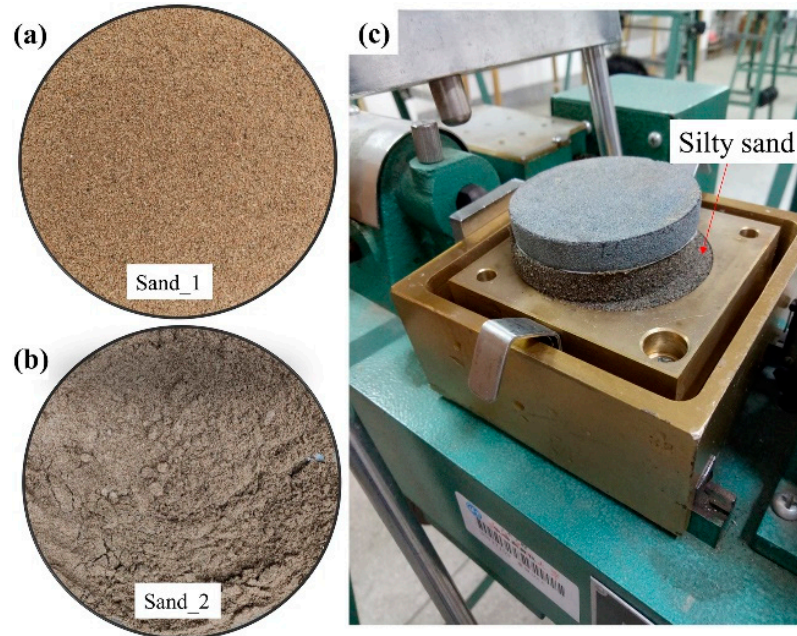

Figure 3. Sand samples and laboratory direct shear test: (**a**) Sand_1; (**b**) Sand_2; (**c**) Laboratory direct shear test.
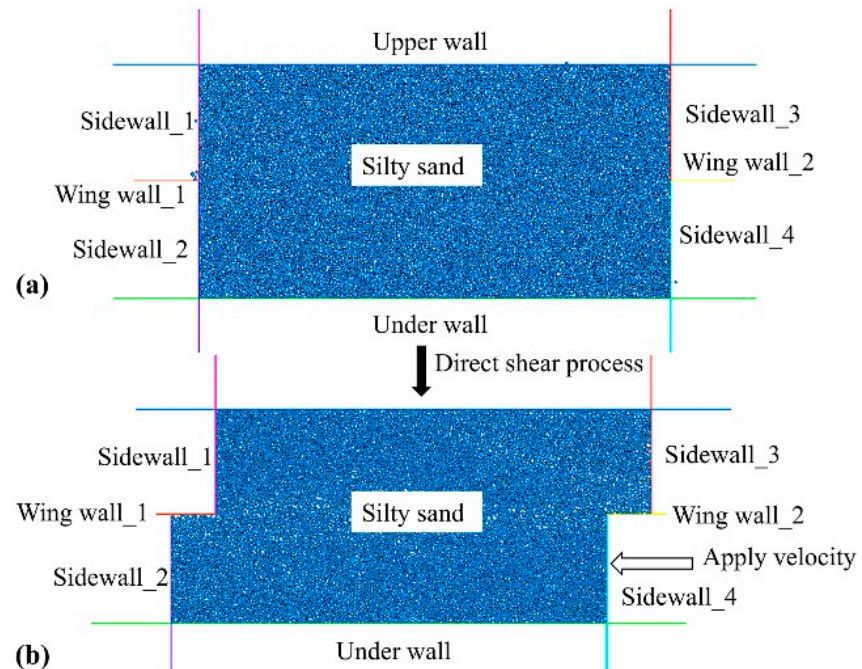

Figure 4. Two states of the direct shear test in two-dimension DEM of silty sand: (**a**) Initial state; (**b**) Final state.
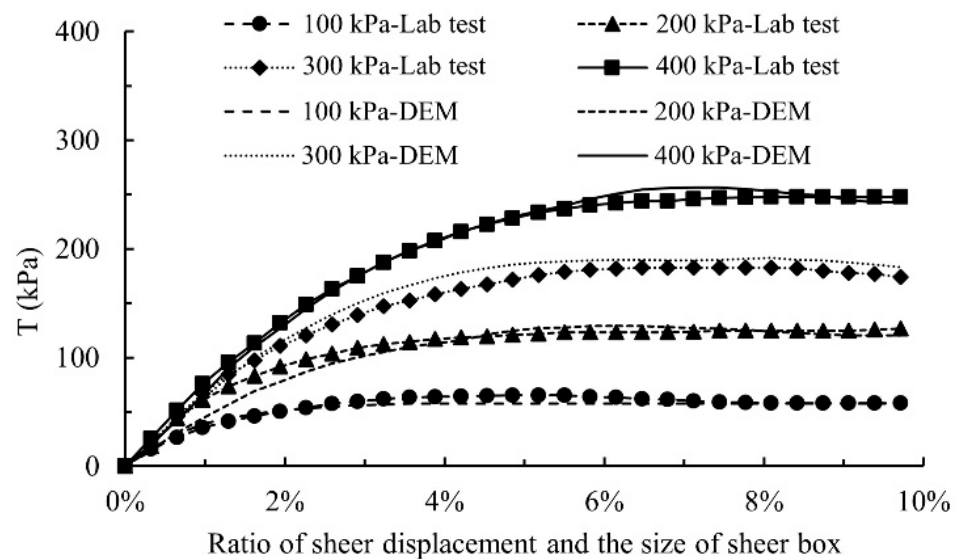
Figure 5. Curve fitting of shear force and shear displacement ratio of silty sand under 100–400 kPa pressure obtained from laboratory direct shear tests and DEM direct shear tests.

C60 concrete was calibrated by triaxial test in DEM [28]. After calibration, the micro-parameters of C60① and C60② concrete are listed in Table 3 [18,29].

4. Twin Tunnels Model in DEM

The establishment process of the DEM model with small diameter (d = 6.2 m) and super-large diameter (D = 15.2 m) twin tunnels are similar. T1 and T2 represent the first and adjacent super-large (D) tunnels, and t1 and t2 are the first and adjacent small (d) tunnels. The outline of small and super-large diameter twin tunnels in DEM is shown in Figure 6. The size of the model is large enough to avoid the boundary effect. [3,28,30] The temperature influence is ignored since the whole time of the train passing the tunnel is 4.18 s. The parameters of the d and D twin tunnels are shown in Table 4. The steps of construction of super-large diameter (D = 15.2 m) twin tunnels model under train vibration is as follows:

Step 1: Four walls are generated as the model's boundary, and the particles with R_1 = 0.12–0.2 m, R_2 = 0.06–0.1 m, and R_3 = 0.02–0.03 m are created inside the area. The particles near the twin tunnels (smaller than 2.0 m) are generated with particles (R_2 = 0.06–0.1 m). Different sizes of particles used in different areas can save calculation time and obtain accurate results. The larger distance between the walls and the tunnel can weaken the boundary effect of the wall to the maximum extent to obtain accurate calculation results. The initial balance state of the model is achieved through calculation, and the initial model is shown in Figure 7a. At this time, all particles in the model adopt the parameters of silty sand.

Step 2: The cross section of super-large diameter twin tunnels as shown in Figure 7b which will built in the red particle region in Figure 7a. First, the geometry, as shown in Figure 7b, was generated; second, redundancies particles inside the D twin tunnel liners are deleted according to the cross-section of the D twin tunnel (Figure 7b); third, micro-parameters of C60 concrete have been used in the red region, as shown in Figure 7c.

Step 3: Gravity and water pressure are set. The lateral pressure coefficient is 0.4. The control conditions of the equilibrium state of the model will be stricter. If the maximum velocity of particles in the model is no more than 0.5 mm/s, the model is considered to reach a balanced state.

Step 4: Measurement circles of the D twin tunnel model are generated as shown in Figure 7d, and the train vibration loads in T1 are simulated by the cosine functions (Figure 2).

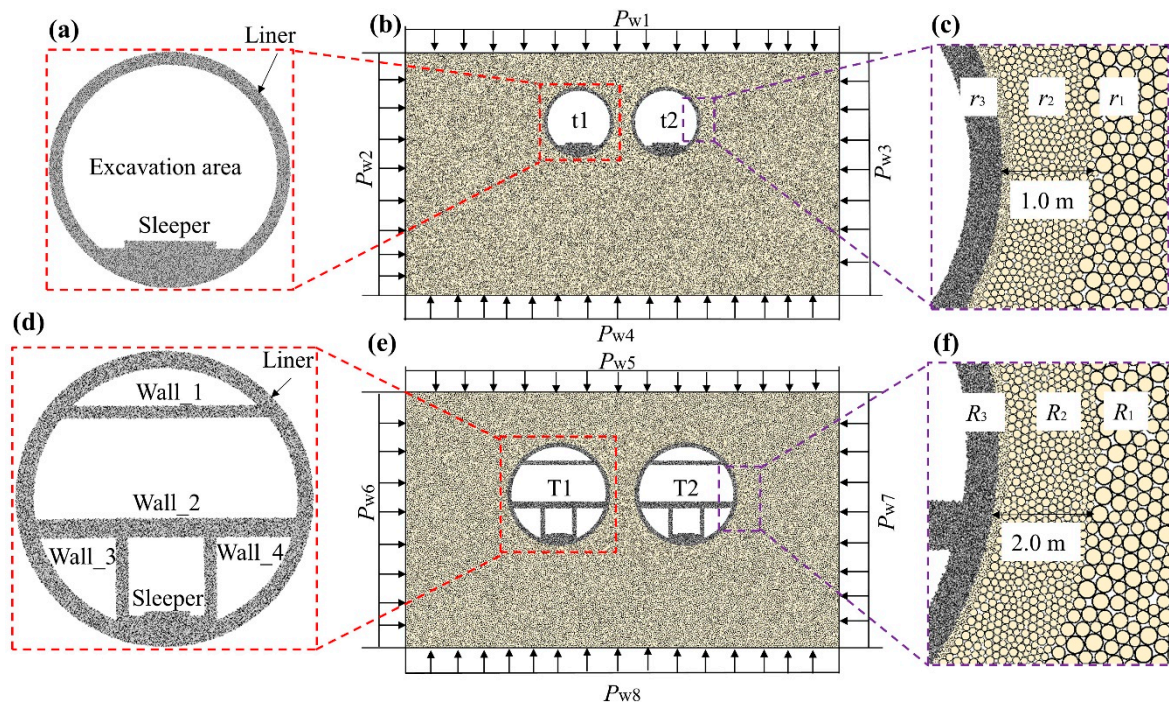The total time of the type A train passing through the twin tunnels at the speed of 120 km/h is 4.18 s.

Figure 6. Small and super-large diameter twin tunnels in DEM: (**a**) Cross section of small tunnel (*d* = 6.2 m); (**b**) Outline of small twin tunnels DEM model; (**c**) The size of particles in the small twin tunnels; (**d**) Cross section of super-large tunnel (*D* = 15.2 m); (**e**) Outline of super-large twin tunnels DEM model; (**f**) The size of particles in the super-large twin tunnels.
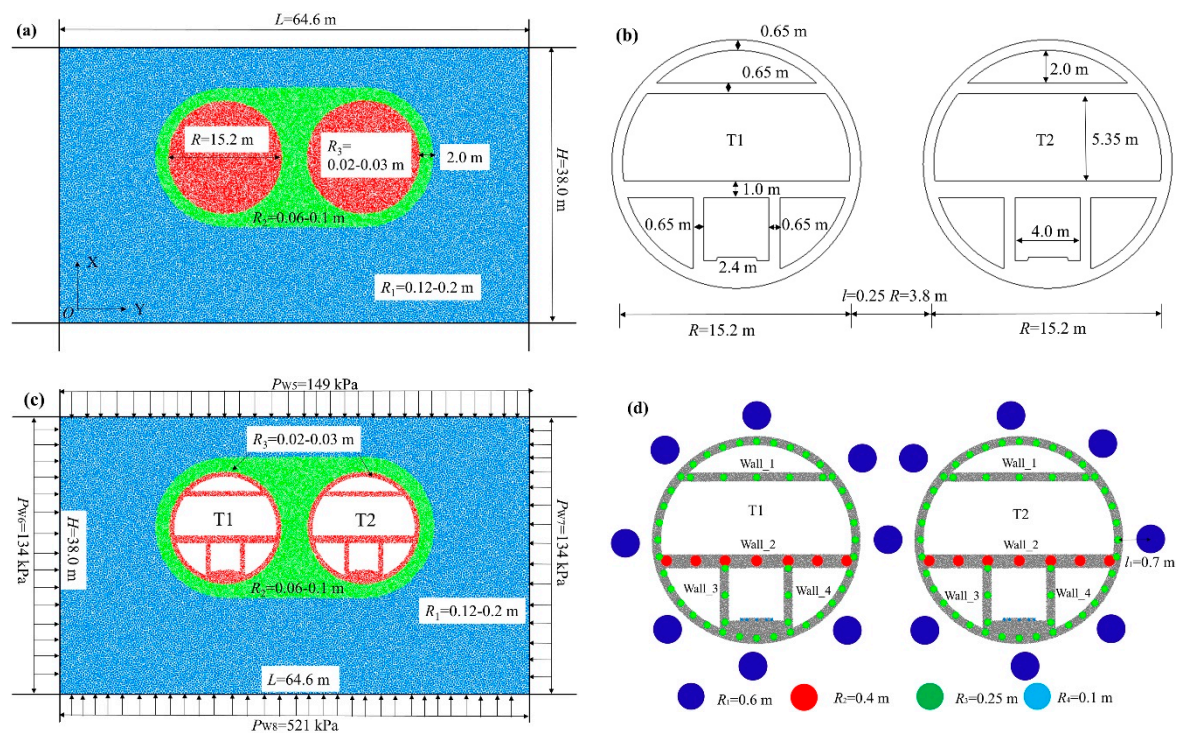

Figure 7. The process of DEM model setup of super-large diameter (*D* = 15.2 m) twin tunnels: (**a**) The initial model of super-large diameter twin tunnels; (**b**) the size of the geometry of super-large diameter twin tunnels; (**c**) the cross-section of super-large diameter twin tunnels; (**d**) detailed layout of monitoring points of the super-large diameter twin tunnels.

Table 4. Parameters of small (*d*) and super-large (*D*) twin tunnels in the DEM model.

Two Types of Twin Tunnels	*d* = 6.2 m	*D* = 15.2 m
Total number of particles	98,008	93,610
Size of whole DEM model (Length × Height) (m)	38.75 × 25.7	64.6 × 38.0
Thickness of liner (m)	0.35	0.65
Water pressure at the top of the model (kPa)	$P_{w1} = 60.8$	$P_{w5} = 149$
Water pressure at the left and right sides of the model (kPa)	$P_{w2} = P_{w3} = 66.8$	$P_{w6} = P_{w7} = 134$
Water pressure at the bottom of the model (kPa)	$P_{w4} = 273.5$	$P_{w8} = 521$
Size of sleeper (Length × Height) (m)	1.2 × 0.2	
Thickness of Wall_1 (m)	-	0.65
Thickness of Wall_2 (m)	-	1.0
Thicknesses of Wall_3 and Wall_4 (m)	-	0.65

5. Results and Discussion

This part is divided into two sections. In section one, the influence of the train vibration on the displacement and velocity of T2 is discussed, such as smoke exhaust board (Wall_1), vehicle lane board (Wall_2), and left and right partition of train track (Wall_3 and Wall_4). In section two, the displacement and velocity of sleepers and liners between t2 and T2 under train vibration are compared. D_H and D_V are horizontal and vertical displacements; V_H and V_V are horizontal and vertical velocities.

5.1. Walls of T2

5.1.1. Smoke Exhaust Board (Wall_1)

Figure 8 shows the displacement and velocity of five measurement points (A_1, B_1, C_1, D_1, 5and E_1) of Wall_1 in T2. D_H of the five measurement points from left to right along with the vibration process of the train (Figure 8a). A positive value of the D_H represents that the Wall_1 moves to the right, while the negative value represents that the Wall_1 moves to the left. After reaching the peak value of horizontal oscillation at about 0.8 s, the amplitude of horizontal oscillation of Wall_1 gradually decreases.
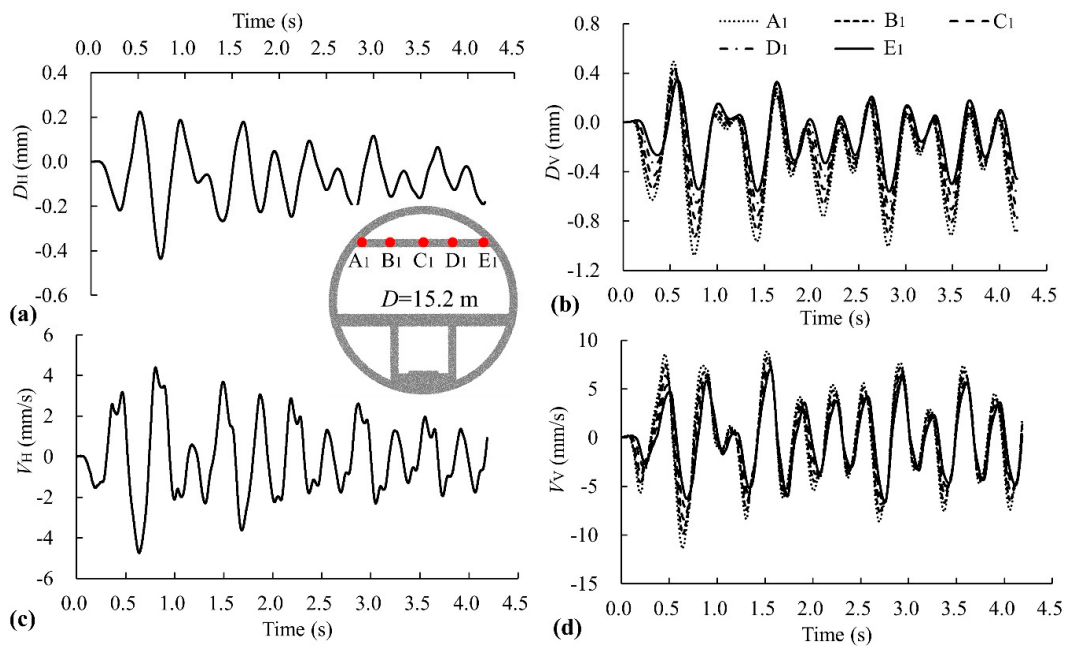

Figure 8. Displacement and velocity of five measurement points (A_1, B_1, C_1, D_1 and E_1) in Wall_1 of T2: (**a**) D_H; (**b**) D_V; (**c**) V_H; (**d**) V_V.

The D_H of Wall_1 is the same, which is possibly related to the larger tension and compression stiffness of Wall_1. The elastic modulus of C60 concrete $E = 3.65$ MPa; the thickness of Wall_1 is 0.65 m, and the supposed width is 1.0 m (so, the cross-sectional area of Wall_1 is 0.65 m^2). Wall_1 of larger tension and compression stiffness ($EA_{W1} = 2.37 \times 10^6$ N/m) has minor deformation so that each measurement point of Wall_1 has the same D_H. The variation law of V_H of the Wall_1 is shown in Figure 8c is very similar to that of D_H, as shown in Figure 8a.

D_V varies during train vibration (Figure 8b). Positive values indicate that the measurement points are moving upward, and the negative values indicate that measurement points are moving downward. After the peak value of vertical oscillation is reached at about 0.8 s, the amplitude of vertical oscillation of the Wall_1 decreases slightly. The negative of the D_V is greater than the positive; this indicates that the downward displacement is larger than the upward displacement of Wall_1. The D_V changes at different monitoring points of the Wall_1 are different, and the left monitoring point near the vibration point is greater than the right monitoring point. The D_V of each measurement point is closely related to the distance between the measurement point and T1.

Compared to Figure 8c,d, the V_V of the Wall_1 is greater than the V_H of the Wall_1, and the V_H and V_V amplitude increases first and then decreases during the whole train operation. The inconsistency between the V_H and V_V of Wall_1 is due to the fact that the train vibration load is vertical, so the disturbance in the vertical direction of Wall_1 is more significant and lasts the whole train vibration process.

According to Figure 8a,d, the displacement and velocity of Wall_1 both reached the maximum at 0.8 s in the train vibration process, and then both decreased slightly with the train vibration process. Therefore, the time point of 0.8 s should be focused on. The stable condition of the model is changed during 0–0.8 s. As a result, the displacement and velocity of the Wall_1 are more significant. The surroundings of the twin tunnel model reach a new stable state gradually after that, which can support the T2 liner so that the displacement and velocity of the Wall_1 are small.

To further compare the differences between the D_V and V_V, the maximum and minimum values of the D_V and V_V of the five measurement points of the Wall_1 are shown in Figure 9. Maximum values of D_V and V_V of the monitoring points-from left to right-decreased slightly, while the minimum values of D_V and V_V increased significantly. Therefore, the maximum and minimum values of D_V and V_V decreased rapidly from left to right. This further validates the pattern found in Figure 8.
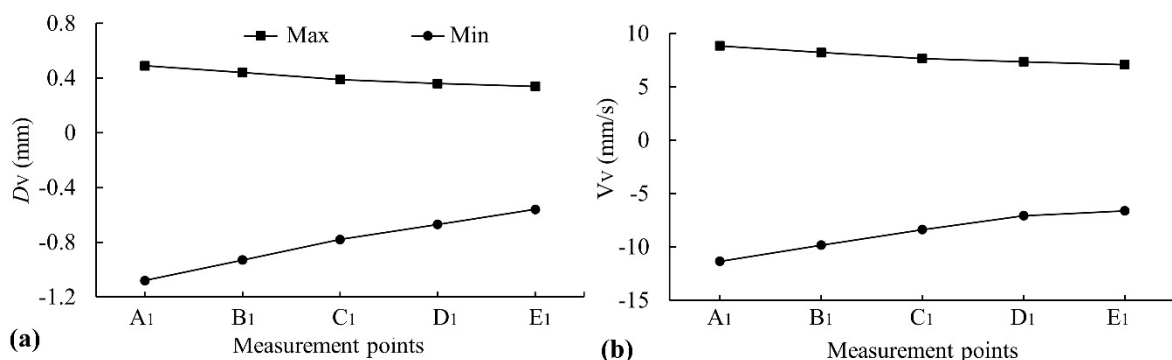

Figure 9. Maximum and minimum value of the D_V and V_V of five measurement points (A_1, B_1, C_1, D_1 and E_1) in Wall_1 of T2: (**a**) maximum and minimum value of the D_V; (**b**) maximum and minimum value of the V_V.

Figures 8 and 9 quantitatively analyze the static and dynamic characteristics of Wall_1s from displacement and velocity in horizontal and vertical directions, respectively. The D_V and V_V of the Wall_1 are greater than the D_H and D_V. The variation law of V_H and V_V is similar to that of D_H and D_V, suggesting that the displacement of the structure can be used as an essential supplementary index for analyzing the dynamic characteristic of T2.

5.1.2. Vehicle Lane Board (Wall_2)

Figure 10 shows the displacement and velocity of seven measurement points (A_2, B_2, C_2, D_2, E_2, F_2 and G_2) of Wall_2 in T2. The variation law of displacement and velocity of Wall_2 is basically the same as that of Wall_1. The D_H of Wall_2 is the same, which means that the tension and compression deformation of Wall_2 is small for the larger tension and compression stiffness ($EA_{W2} = 3.65 \times 10^6$ N/m), which is similar to the law of Wall_1. The more extensive D_V at the left side of Wall_2 is caused by the near distance to the train vibration position.
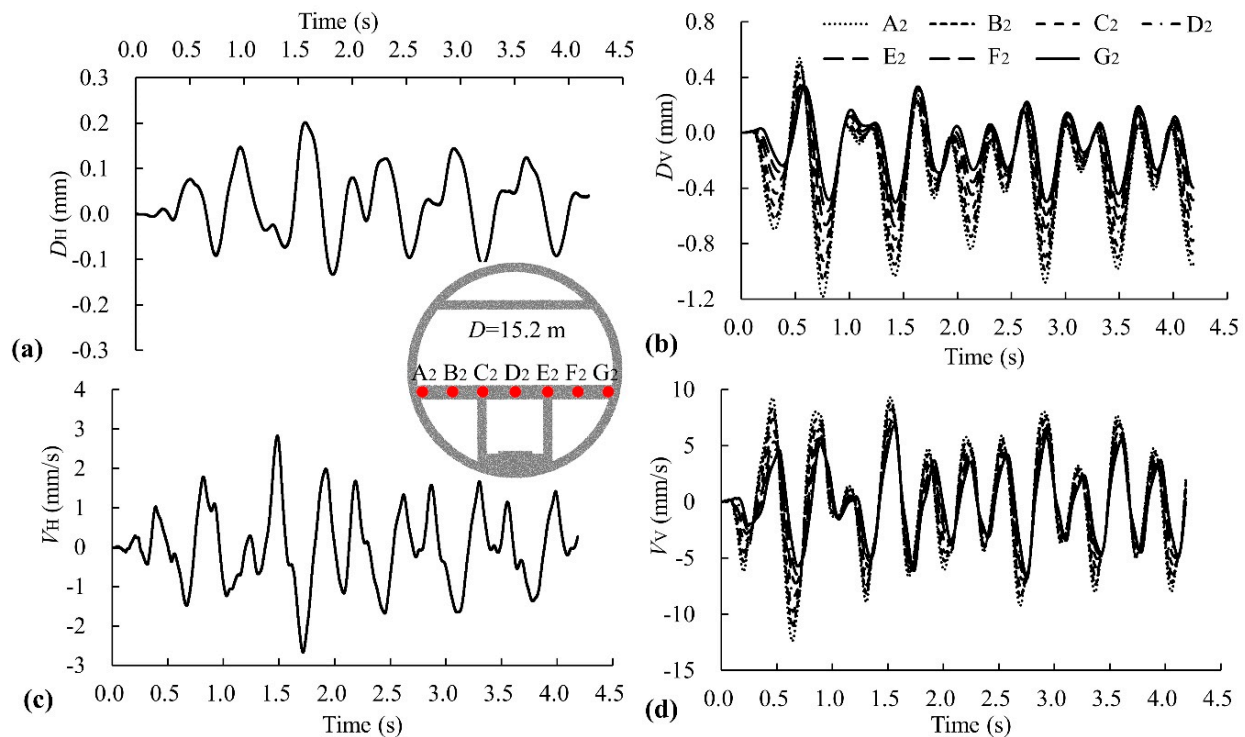

Figure 10. Displacement and velocity of seven measurement points (A_2, B_2, C_2, D_2, E_2, F_2 and G_2) in Wall_2 of T2: (**a**) D_H; (**b**) D_V; (**c**) V_H; and (**d**) V_V.

D_H of Wall_1 is much larger than that of Wall_2 (Figures 8a and 10a). Wall_1 is located in the upper part of the cross-section in T2, and Wall_2 is located in the middle part of the cross-section in T2. Soil stress in the horizontal direction (stress-xx) around the two sides of Wall_1 is 1.90×10^5 and -1.28×10^6, and soil stress in the horizontal direction (stress-xx) around the two sides of Wall_2 are 4.09×10^6 and -3.57×10^6. Soil stress in the vertical direction (stress-yy) around the two sides of Wall_1 is -1.16×10^6 and -7.72×10^5, and soil stress in the vertical direction (stress-yy) around the two sides of Wall_2 is 1.76×10^6 and -4.46×10^6. The stress around Wall_1 is smaller than Wall_2, so Wall_1 has larger D_H for smaller limitations. The stress state of surroundings significantly affects the D_H of Wall_1 and Wall_2.

The D_V of Wall_2 is greater than that of Wall_1 at the midpoint (Figures 8b and 10b) as Wall_2 is close to the train vibration in T1. Therefore, the D_V of the walls is much affected by distance while less affected by surroundings extrusion.

Maximum and minimum values of the D_V and V_V of the seven measurement points of the Wall_2 are shown in Figure 11. The D_V and V_V decrease from point A_2 to point G_2. The variation law of D_V and V_V in Wall_2 conform to the law of "near is large and far is small".
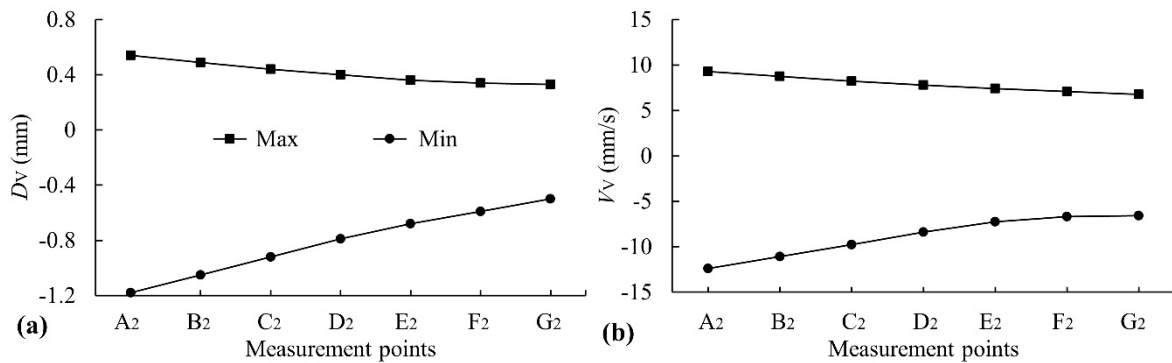
Figure 11. Maximum and minimum value of the D_V and V_V of seven measurement points (A$_2$, B$_2$, C$_2$, D$_2$, E$_2$, F$_2$, and G$_2$) in Wall_2 of T2: (**a**) maximum and minimum value of the D_V; (**b**) maximum and minimum value of the V_V.

5.1.3. Left and Right Partition of Train Track (Wall_3 and Wall_4)

Figure 12 compares the horizontal displacement and velocity of Wall_3 and Wall_4 in T2. The variation law of D_H and V_H of Wall_3 and Wall_4 is basically the same. The negative value of D_H is basically the same at the monitoring points of different heights, but the positive D_H gradually increases. The peak-peak value of D_H of Wall_3 and Wall_4 decreases from top to bottom (Figure 12a), possibly related to the combined influence of the stress of surroundings around T2 and the distance between monitoring points and vibration position. The D_H of Wall_3 and Wall_4 is smaller than that of Wall_1 and Wall_2, as Wall_3 and Wall_4 are lower and have more considerable surrounding stress.
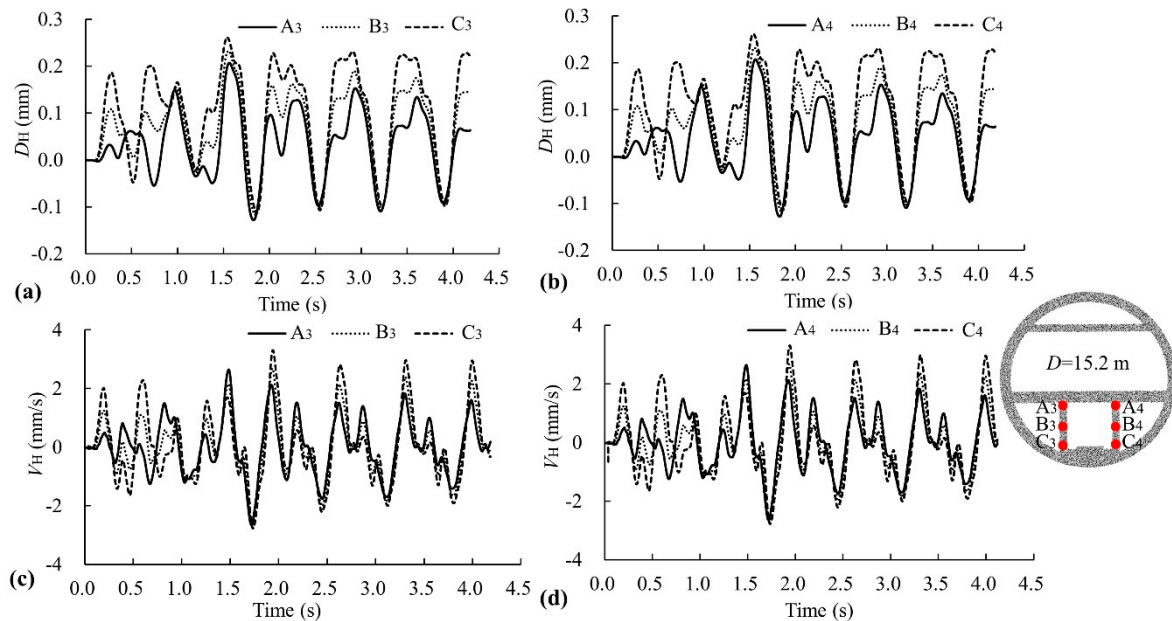

Figure 12. Horizontal displacement and velocity of Wall_3 and Wall_4 in T2: (**a**) D_H of Wall_3; (**b**) D_H of Wall_4; (**c**) D_V of Wall_3; and (**d**) D_V of Wall_4.

Figure 13 shows the D_V and V_V of Wall_3 and Wall_4 in T2. The D_V of Wall_3 is slightly larger than that of Wall_4, as Wall_3 is closer to the train vibration point of T1. Each measurement point of Wall_3 and Wall_4 has the same D_V (Figure 13a,b) due to the larger tension and compression stiffness ($EA_{W3} = EA_{W4} = 2.37 \times 10^6$ N/m).
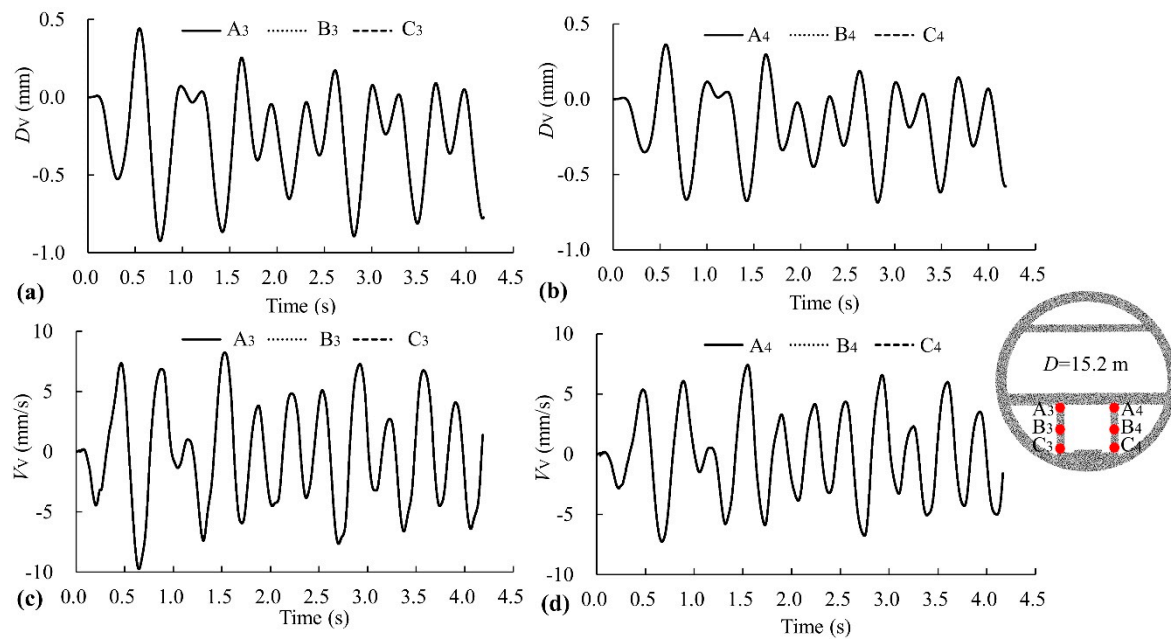
Figure 13. Vertical displacement and velocity of Wall_3 and Wall_4 in T2: (**a**) D_V of Wall_3; (**b**) D_V of Wall_4; (**c**) V_V of Wall_3; and (**d**) V_V of Wall_4.

Figures 8–13 show that all inner walls (Wall_1, Wall_2, Wall_3, and Wall_4) experienced oscillatory movement both in the horizontal and vertical direction during train vibration. Vertical displacement and velocity are more remarkable than horizontal displacement and velocity. The horizontal walls (Wall_1 and Wall_2) have the same horizontal displacement, and the vertical walls (Wall_3 and Wall_4) have the same vertical displacement. D_H decreases gradually from top to bottom because the silty sand stress rises. D_V increases gradually from top to bottom because the measurement point is closer to the train vibration point. The variation law of V_H and V_V is similar to that of D_H and D_V, suggesting that the displacement of the structure can be used as an essential supplementary index for analyzing the dynamic characteristic of T2.

5.2. Comparison of t2 and T2

5.2.1. Sleeper

Figure 14 compares the displacement and velocity of sleepers between t2 and T2. Monitoring points S_2 and S_4 are the points of trains load in T2. Displacement and velocity of the two monitoring points (S_2 and S_4) of the t2 sleeper basically coincide, and the displacement and velocity of the T2 sleeper also coincide. Therefore, four monitoring points are compared in this figure, while only two curves can be seen intuitively in each sub-figure.

D_H of t2 and T2 oscillates in the left and right directions during train vibration (Figure 14a). The amplitude of D_H of t2 and T2 gradually increases between 0 s and 1.3 s, and then the amplitude of D_H basically remains unchanged. After that, the peak-peak values of the D_H of t2 and T2 are very similar. Therefore, the D_H of t2 and T2 are basically not affected by the size of diameter, and the peak-peak value of t2 and T2 is less than 0.35 mm. The D_H of t2 and T2 has a small response in the train vibration process.

Compared to Figure 14a,c, V_H of T2 is smaller than that of t2. The dynamic response of T2 in the horizontal direction is smaller than that of t2, and T2 is more stable than t2 in the horizontal direction.

D_V of t2 and T2 oscillates in the upward and downward directions during train vibration (Figure 14b). D_V of t2 is much larger than that of T2. The peak-peak value of the D_V of t2 is about 1.9 mm, and the peak-peak value of the D_V of T2 is about 1.1 mm. Therefore, the vertical displacement of t2 is about two times that of T2.
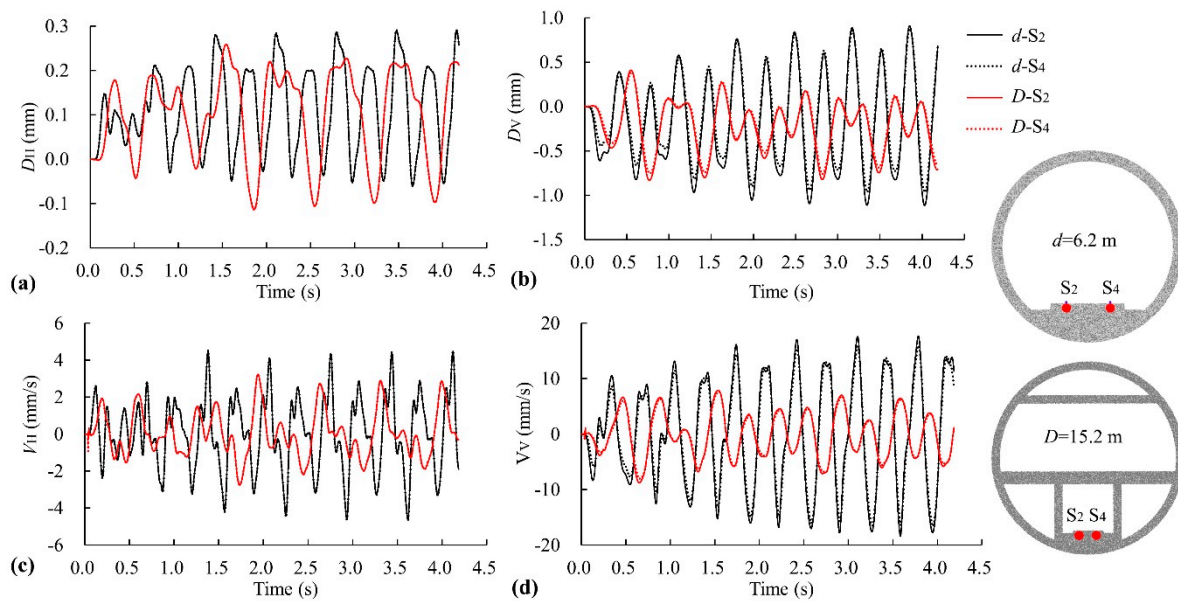
Figure 14. Displacement and velocity of sleepers between t2 and T2: (**a**) D_H; (**b**) D_V; (**c**) V_H; and (**d**) V_V.

The amplitude of the D_V of the t2 gradually increases between 0 s and 2.7 s, and then the amplitude of the D_V basically remains unchanged. Therefore, the t2 sleeper reaches a new equilibrium state at about 2.7 s, and the t2 tends to be in dynamic equilibrium. The vibration amplitude of the D_V of the T2 increases gradually from 0 s to 0.8 s and decreases gradually from 0.8 to 1.7 s. Subsequently, the vibration amplitude of the D_V of the T2 is stable in the region. It can be seen that the T2 gradually reaches the equilibrium state between 0.8 and 1.7 s. Compared with the small-diameter tunnel, the time needed to reach the new equilibrium state in the train vibration process in the super-large diameter tunnel is shorter (2.7 s) than that in the small-diameter tunnel. This shows that the super-large diameter tunnel is more stable than the small-diameter tunnel in the train vibration process. Therefore, it can be seen that T2 is more stable than t2 from two aspects: the time of the tunnel reaches the equilibrium state and the amplitude of D_V.

Compared to Figure 14b,d, the laws of D_V and V_V of t2 and T2 are basically similar. The peak-peak of the V_V of the t2 is about 37 mm/s, and the peak-peak of the V_V of the T2 is about 17 mm/s, and the V_V of the t2 is about two times that of the T2.

According to Figure 14a,d, the sleeper in t2 and T2 will occur the horizontal and vertical vibration displacement and velocity during the train running in T1. In general, the displacement and velocity of t2 are more significant than those of T2.

The responses of D_V and V_V in t2 and T2 are greater than those of horizontal directions. The vertical response of the structure should be paid more attention to the process of train vibration. T2 is more stable than t2 from two aspects: the time of the tunnel reaches the equilibrium state and the vibration amplitude of the structure's dynamic and static response. The dynamic characteristics of the D twin tunnels are very different from those of the d twin tunnels, so the dynamic characteristics of the train vibration in the d twin tunnels cannot be directly applied to the D twin tunnels.

5.2.2. Liner

Figure 15 compares the resultant displacement of the t2 and T2 liner, and the measurement points are shown in Figure 15b,c. The resultant displacement is the arithmetic square root of the D_H and D_V. The resultant displacement on the left side of the t2 liner is greater than that on the right side; the maximum value on the left side is about 1.24 mm at 180°, and the minimum value on the right side is about 0.82 mm at 0°. The resultant displacement of the T2 liner is also greater on the left side than on the right side; the maximum value on the left side is about 1.2 mm at 180°, and the minimum value on the

right side is about 0.25 mm at 0°. Therefore, the resultant displacement of the left liner of t2 and T2 is large, and the values are close to each other. The resultant displacement of the right side of the liner is small, while the difference of the resultant displacement of the right side of the liner in the t2 and T2 is large.
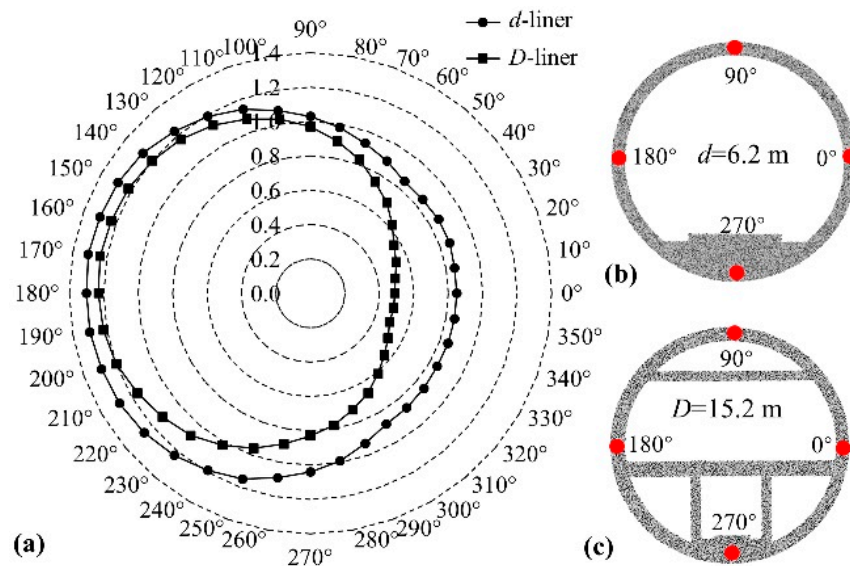

Figure 15. Comparison of resultant displacement of t2 and T2: (**a**) maximum value of resultant displacement; (**b**) measurement points of t2; (**c**) measurement points of T2.

The resultant displacement on the right side of the t2 liner is much larger than that of the T2 liner. The possible reason for this is the fact that the distance between the monitoring point of the right-side liner of the T2 and the vibration point of the train in T1 is very large. The energy dissipation of the vibration wave of the train is basically completed. The research results of *d* tunnel can not be directly applied to the engineering of the *D* tunnel; it is necessary to strengthen the related research of the super-large diameter tunnel.

Figure 16 shows the comparison of maximum and average values of resultant velocities between t2 and T2. The maximum and average values of the velocity in t2 and T2 have basically the same variation rule, both of which are larger on the left side of the liner and smaller on the right side of the liner. Moreover, the velocity of the T2 is about 50% of that value of the t2; this indicates that the *D* twin tunnel is more stable than the *d* twin tunnel, which may be the result of the joint action of the larger space between the *D* twin tunnels and the greater water pressure around *D* twin tunnels. In addition, different sections of small and super-large diameter twin tunnels may also play an important role. The super-large twin tunnels have been stiffer due to the inner walls (Wall_1, Wall_2, Wall_3, and Wall_4) were added to them.

Horizontal stress (σ_x) and vertical stress (σ_y) of liner in t2 and T2 can be seen in Figure 17. Positive values represent tensile stresses, and negative values represent compressive stresses. The absolute value of σ_x at 0° and 180° of T2 liner are greater than that of the t2 liner, and the variation amplitude of σ_x is smaller in the train vibration process (Figure 17a). The change of σ_y at 90° and 270°is similar to that of σ_y in t2 and T2 (Figure 17b). In addition, special attention needs to be paid to the monitoring points where the tunnel liner exhibits high tensile strength, as the concrete liner has a strong compressive strength and a weak tensile strength.
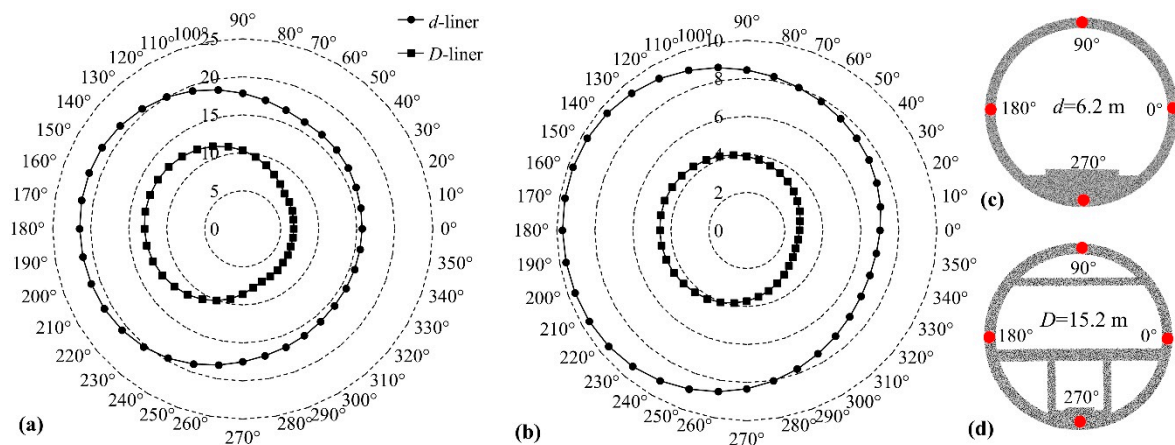
Figure 16. Comparison of resultant velocity of t2 and T2: (**a**) maximum value of resultant velocity; (**b**) average value of resultant velocity; (**c**) measurement points of t2; (**d**) measurement points of T2.
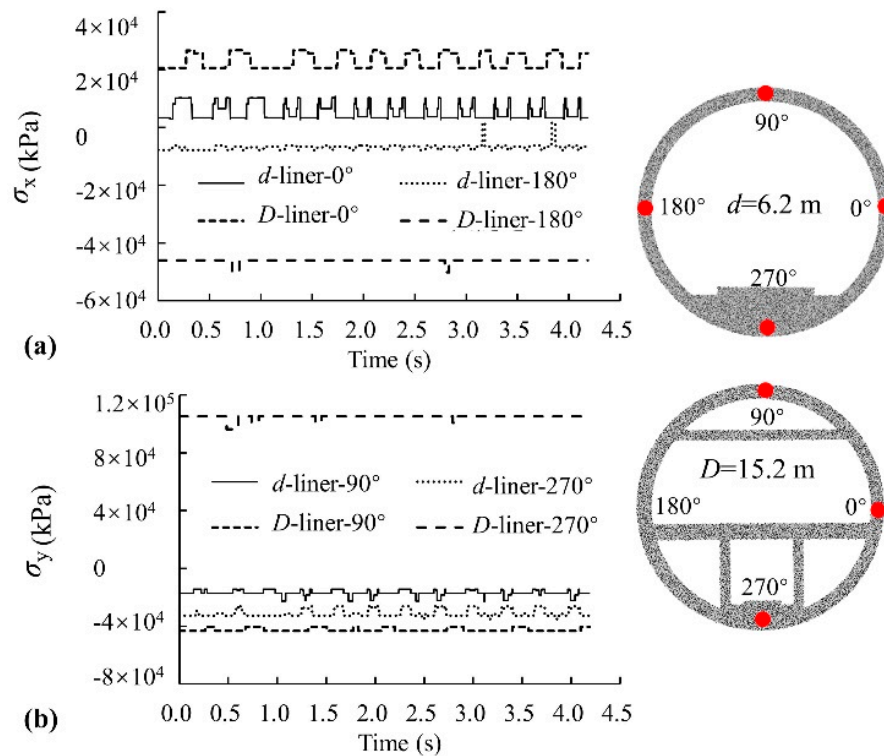

Figure 17. Horizontal and vertical stress of liner in t2 and T2: (**a**) Horizontal stress (σ_x); (**b**) Vertical stress (σ_y).

Figure 18 shows the cloud of the resultant velocity of the liner in t2 and T2 at some key time points. The resultant velocity at each time point of the tunnel is related to the dynamic load of the train, and the resultant velocity on the left side of the liner is larger than the value on the left side both in t2 and T2. The resultant speed of the super-large diameter tunnel is obviously less than that of the small-diameter tunnel, which means the stability of the super-large diameter tunnel is better than the small-diameter tunnel.
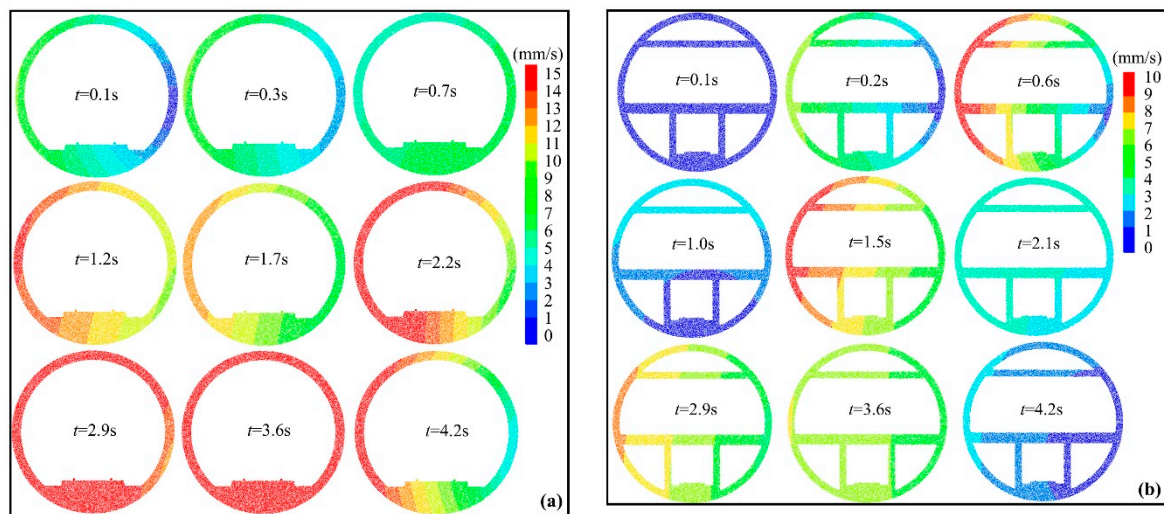
Figure 18. Cloud of the resultant velocity of liner in t2 and T2: (**a**) Resultant velocity of t2 liner at key time points; (**b**) Resultant velocity of T2 liner at key time points.

6. Conclusions

This paper presents DEM dynamic analysis results of small (d = 6.2 m) and super-large (D = 15.2 m) diameter twin tunnels during a train's vibration at a speed of 120 km/h in T1. Velocity and displacement of T2 walls are discussed, and the sleeper and liner of t2 and T2 are compared. The main conclusions are as follows:

1. Four walls (Wall_1, Wall_2, Wall_3, and Wall_4) vibrate in horizontal and vertical directions. The D_H and V_V are more significant than the D_H and V_H. The horizontal structure (Wall_1 and Wall_2) has the same D_H, and the vertical structure (Wall_3 and Wall_4) has the same D_V. The stress state of the surroundings around T2 is a decisive factor for D_H, and the distance from the vibration point to the measurement point is the decisive factor for the D_V.

2. The super-large and small tunnel sleepers will have oscillating displacement and velocity in the horizontal and vertical directions. The resultant displacement and velocity at the left side of t2 and T2 liners are more significant than on the right. The resultant displacement of the right side of the liner is small, and the difference of the resultant displacement of the right side of the liner in the t2 and T2 is significant. In general, the displacement and velocity of the d tunnel are more significant than those of the D tunnel. The D_V and V_V of t2 and T2 liners are greater than those of D_H and V_H. Therefore, the vertical response of the structure should be paid more attention to during the process of train vibration.

3. The law of the V_H and V_V is similar to that of the D_H and D_V, indicating that displacement analysis can supplement dynamic structural analysis. T2 is more stable than t2 from two aspects, namely the time of the tunnel reaches the equilibrium state and the vibration amplitude of the structure's dynamic and static response. This possibility is the result of super-large diameter twin tunnel spacing, high upper water pressure and more stable cross-section.

Dynamic characteristics of t2 and T2 during train vibration are significantly different, so the dynamic characteristics in d twin tunnels cannot be applied directly to the D twin tunnels. The two-dimensional DEM model can explore the dynamic characteristics of small and super-large twin tunnels under train vibration.

Author Contributions: Conceptualization, L.W. and X.Z.; methodology, W.W.; software, L.W.; validation, L.W., W.W., and X.M.; formal analysis, W.W.; investigation, H.G.; resources, H.G.; data curation, L.W.; writing—original draft preparation, L.W.; writing—review and editing, W.W.; visualization, X.M.; supervision, X.Z. All authors have read and agreed to the published version of the manuscript.

References

1. Zhang, Z.H.; Zhang, X.D.; Cui, Y.F.; Qiu, H.S. Discrete element modeling of a cross-river tunnel under subway train operation during peak and off-peak periods. *Arab. J. Geosci.* **2019**, *12*, 102. [CrossRef]
2. Li, S.; Li, P.; Zhang, M.; Liu, Y. Influence of Approaching Excavation on Adjacent Segments for Twin Tunnels. *Appl. Sci.* **2020**, *10*, 98. [CrossRef]
3. Wu, L.; Zhang, X.; Kuang, F.; Sui, J.; Xilong, Z.; Guo, H. Dynamic characteristics of adjacent tunnel and surroundings under the vibration of trains in the first tunnel with different buried depths. *Arab. J. Sci. Eng.* **2021**, *46*, 5105–5119. [CrossRef]
4. Xie, X.; Yang, Y.; Ji, M. Analysis of ground surface settlement induced by the construction of a large-diameter shield-driven tunnel in Shanghai, China. *Tunn. Undergr. Space Technol.* **2016**, *51*, 120–132. [CrossRef]
5. Ağbay, E.; Topal, T. Evaluation of twin tunnel-induced surface ground deformation by empirical and numerical analyses (NATM part of Eurasia tunnel, Turkey). *Comput. Geotech.* **2020**, *119*, 103367. [CrossRef]
6. Yertutanol, K.; Akgün, H.; Sopacı, E. Displacement monitoring, displacement verification and stability assessment of the critical sections of the Konak tunnel, İzmir, Turkey. *Tunn. Undergr. Space Technol.* **2020**, *101*, 103357. [CrossRef]
7. Zhang, F.; Gao, Y.; Wu, Y.; Wang, Z. Face stability analysis of large-diameter slurry shield-driven tunnels with linearly increasing undrained strength. *Tunn. Undergr. Space Technol.* **2018**, *78*, 178–187. [CrossRef]
8. Fuyong, C.; Lin, W.; Wengang, Z. Reliability assessment on stability of tunnelling perpendicularly beneath an existing tunnel considering spatial variabilities of rock mass properties. *Tunn. Undergr. Space Technol.* **2019**, *88*, 276–289. [CrossRef]
9. Zhang, J.; Yuan, Y.; Yu, H. Shaking table tests on discrepant responses of shaft-tunnel junction in soft soil under transverse excitations. *Soil Dyn. Earthq. Eng.* **2019**, *120*, 345–359. [CrossRef]
10. Sun, B.; Deng, M.; Zhang, S.; Cui, W.; Wang, C.; Yu, L.; Cao, K. Inelastic dynamic analysis and damage assessment of a hydraulic arched tunnel under near-fault SV waves with arbitrary incoming angles. *Tunn. Undergr. Space Technol.* **2020**, *104*, 103523. [CrossRef]
11. Yan, L.; Haider, A.; Li, P.; Song, E. A numerical study on the transverse seismic response of lined circular tunnels under obliquely incident asynchronous P and SV waves. *Tunn. Undergr. Space Technol.* **2020**, *97*, 103235. [CrossRef]
12. Huang, Q.; Huang, H.-W.; Ye, B.; Zhang, D.-m.; Gu, L.-l.; Zhang, F. Dynamic response and long-term settlement of a metro tunnel in saturated clay due to moving train load. *Soils Found.* **2017**, *57*, 1059–1075. [CrossRef]
13. Yang, Y.B.; Liang, X.; Hung, H.-H.; Wu, Y. Comparative study of 2D and 2.5D responses of long underground tunnels to moving train loads. *Soil Dyn. Earthq. Eng.* **2017**, *97*, 86–100. [CrossRef]
14. He, C.; Zhou, S.; Di, H.; Shan, Y. A 2.5-D coupled FE–BE model for the dynamic interaction between saturated soil and longitudinally invariant structures. *Comput. Geotech.* **2017**, *82*, 211–222. [CrossRef]
15. He, C.; Zhou, S.; Di, H.; Guo, P.; Xiao, J. Analytical method for calculation of ground vibration from a tunnel embedded in a multi-layered half-space. *Comput. Geotech.* **2018**, *99*, 149–164. [CrossRef]
16. Yang, W.B.; Cui, G.; Xu, Z.Y.; Yan, Q.X.; He, C.; Zhang, Y.Y. An experimental study of ground-borne vibration from shield tunnels. *Tunn. Undergr. Space Technol.* **2018**, *71*, 244–252. [CrossRef]
17. Yang, W.; Zhang, C.; Liu, D.; Tu, J.; Yan, Q.; Fang, Y.; He, C. The effect of cross-sectional shape on the dynamic response of tunnels under train induced vibration loads. *Tunn. Undergr. Space Technol.* **2019**, *90*, 231–238. [CrossRef]
18. Zhang, Z.H.; Zhang, X.D.; Tang, Y.; Cui, Y.F. Discrete element analysis of a cross-river tunnel under random vibration levels induced by trains operating during the flood season. *J. Zhejiang Univ. A* **2018**, *19*, 346–366. [CrossRef]
19. Ding, D.-Y.; Liu, W.-N.; Gupta, S.; Lombaert, G.; Degrande, G. Prediction of vibrations from underground trains on Beijing metro line 15. *J. Cent. S. Univ.* **2010**, *17*, 1109–1118. [CrossRef]
20. Yan, Q.; Chen, H.; Chen, W.; Zhang, J.; Ma, S.; Huang, X. Dynamic Characteristic and Fatigue Accumulative Damage of a Cross Shield Tunnel Structure under Vibration Load. *Shock Vib.* **2018**, *2018*, 9525680. [CrossRef]
21. Yan, Q.; Song, L.; Chen, H.; Chen, W.; Ma, S.; Yang, W. Dynamic Response of Segment Lining of Overlapped Shield Tunnels Under Train-Induced Vibration Loads. *Arab. J. Sci. Eng.* **2018**, *43*, 5439–5455. [CrossRef]
22. Zhao, Y.; Shi, Y.; Yang, J. Study of the Influence of Train Vibration Loading on Adjacent Damaged Tunnel. *Shock Vib.* **2019**, *2019*, 3417598. [CrossRef]
23. He, C.; Zhou, S.; Guo, P.; Di, H.; Zhang, X. Modelling of ground vibration from tunnels in a poroelastic half-space using a 2.5-D FE-BE formulation. *Tunn. Undergr. Space Technol.* **2018**, *82*, 211–221. [CrossRef]
24. He, C.; Zhou, S.; Guo, P.; Di, H.; Zhang, X. Analytical model for vibration prediction of two parallel tunnels in a full-space. *J. Sound Vib.* **2018**, *423*, 306–321. [CrossRef]

25. Zhou, S.; He, C.; Guo, P.; Di, H.; Zhang, X. Modeling of Vehicle-Track-Tunnel-Soil System Considering the Dynamic Interaction between Twin Tunnels in a Poroelastic Half-Space. *Int. J. Geomech.* **2020**, *20*, 04019144. [CrossRef]

26. Zhou, C.; Luo, H.; Fang, W.; Wei, R.; Ding, L. Cyber-physical-system-based safety monitoring for blind hoisting with the internet of things: A case study. *Automat. Constr.* **2019**, *97*, 138–150. [CrossRef]

27. Zhang, Z.H.; Zhang, X.D.; Qiu, H.S.; Daddow, M. Dynamic characteristics of track-ballast-silty clay with irregular vibration levels generated by high-speed train based on DEM. *Constr. Build. Mater.* **2016**, *125*, 564–573. [CrossRef]

28. Wu, L.; Zhang, X.; Zhang, Z.; Sun, W. 3D Discrete Element Method Modelling of Tunnel Construction Impact on an Adjacent Tunnel. *KSCE J. Civ. Eng.* **2020**, *24*, 657–669. [CrossRef]

29. Itasca. *Particle Flow Code in 2 Dimensions (PFC2D). User's Guide*; Itasca Consulting Group: Minneapolis, MN, USA, 2004.

30. Maynar, M.J.; Rodríguez, L.E. Discrete Numerical Model for Analysis of Earth Pressure Balance Tunnel Excavation. *J. Geotech. Geoenviron. Eng.* **2005**, *131*, 1234–1242. [CrossRef]